AGU ADVANCING EARTH AND SPACE SCIENCE

Geophysical Research Letters

RESEARCH LETTER
10.1029/2020GL091508

Mercury Evidence of Intense Volcanism Preceded Oceanic Anoxic Event 1d

Hanwei Yao[1], Xi Chen[1], Runsheng Yin[2], Stephen E. Grasby[3], Helmut Weissert[4], Xue Gu[1], and Chengshan Wang[1]

[1]State Key Laboratory of Biogeology and Environmental Geology, China University of Geosciences, Beijing, China, [2]State Key Laboratory of Ore Deposit Geochemistry, Institute of Geochemistry, Chinese Academy of Sciences, Guiyang, China, [3]Geological Survey of Canada, Natural Resources Canada, Calgary, Canada, [4]Department of Earth Sciences, Geological Institute, Zürich, Switzerland

Key Points:

- The first mercury (Hg) concentration and isotope record of Oceanic Anoxic Event (OAE) 1d, from southern Tibet
- Hg anomaly prior to the onset of OAE 1d is derived from a volcanic source
- Central Kerguelen LIP volcanism may have triggered OAE 1d global climate change

Supporting Information:

- Supporting Information S1
- Table S1
- Table S2
- Table S3

Correspondence to:

X. Chen and R. Yin,
xichen@cugb.edu.cn;
yinrunsheng@mail.gyig.ac.cn

Citation:

Yao, H., Chen, X., Yin, R., Grasby, S. E., Weissert, H., Gu, X., & Wang, C. (2021). Mercury evidence of intense volcanism preceded oceanic anoxic event 1d. *Geophysical Research Letters*, *48*, e2020GL091508. https://doi.org/10.1029/2020GL091508

Received 2 NOV 2020
Accepted 5 FEB 2021

Abstract Geochemical studies of marine sediments indicate that most Oceanic Anoxic Events (OAEs) appear coincident with Large Igneous Province (LIP) volcanism. OAE 1d records peculiar paleoceanographic changes and global carbon cycle perturbations, however, its association with volcanism has not yet been supported by robust geochemical evidence. To examine the potential role of volcanism we investigated the mercury (Hg) concentration and isotopic record of OAE 1d interval at the Youxia section, southern Tibet. The interval prior to OAE 1d is marked by a combined positive Δ^{199}Hg and Hg content shift, which suggests a volcanic Hg source. These findings are consistence with a prominent increase in sea surface temperatures and atmospheric CO_2 before OAE 1d. We suggest that eruption of the central portion of the Kerguelen LIP may have been the main source of the Hg anomaly and resulted in global environment perturbations that drove the onset of the anoxia event.

Plain Language Summary The mid-Cretaceous is characterized by globally high temperature, sea-level, and atmospheric CO_2. Recurrent volcanism considered to be the main driver of the Cretaceous hothouse, led also to frequent ocean anoxia events and global carbon cycle perturbations. One such perturbation is oceanic anoxic event (OAE) 1d; however, unlike other OAEs its association with volcanism has not yet been proven. Mercury (Hg) is mainly sourced from volcanism, and enhanced volcanic activity is recorded as spikes in Hg concentration in marine sediments. We used multiple geochemical proxies, especially Hg chemical analyses, to examine the potential role of volcanism in the OAE 1d event. Based on the data, we find a volcanic derived Hg anomaly occurred just prior to the onset of the OAE. These findings are in agreement with a prominent increase in sea surface temperatures and atmospheric CO_2 at the same period. We suggest then that the eruption of the central portion of Kerguelen LIP resulted in global environment perturbations that drove the onset of the OAE 1d.

1. Introduction

Mesozoic Oceanic Anoxic Events (OAEs, Schlanger and Jenkyns, 1976) mark times of major changes to global climate and marine systems, along with major perturbations in the global carbon cycle (Jenkyns, 2010). Globally enhanced deposition of marine organic-rich black shales are associated with carbon isotope excursions of marine sediments during OAEs (Weissert, 1989). Elevated productivity at times when oceans were fertilized with biolimiting elements and metals (Leckie et al., 2002), and widespread low oxygen concentrations in restricted basins, favored the deposition of large amounts of organic matter (Sinton & Duncan, 1997). OAE 1 d preceded the Albian-Cenomanian boundary (~100.5 Ma; Ogg et al., 2012) by about ~300 kyr (Yao et al., 2018) and it is characterized by a perturbation of the global carbon cycle as recorded in C-isotope stratigraphy, by changes of upper ocean water temperature in the western Tethys and the Atlantic (Bornemann et al., 2005; Wilson & Norris, 2001), as well as widespread oceanographic and depositional changes in the western Tethys (Giorgioni et al., 2015). Reconstruction of atmospheric pCO_2 during OAE 1d indicates that OAE 1d coincides with elevated pCO_2 similar to OAE 2 and shared a possible causal or developmental mechanism with OAE 1a and the Toarcian OAE (T-OAE), both of which are thought to be triggered by Large Igneous Province (LIP) volcanism (Richey et al., 2018). However, to date conclusive geochemical evidence of the link between OAE 1d and volcanism is absent, leaving it as an anomalous Mesozoic OAE event.

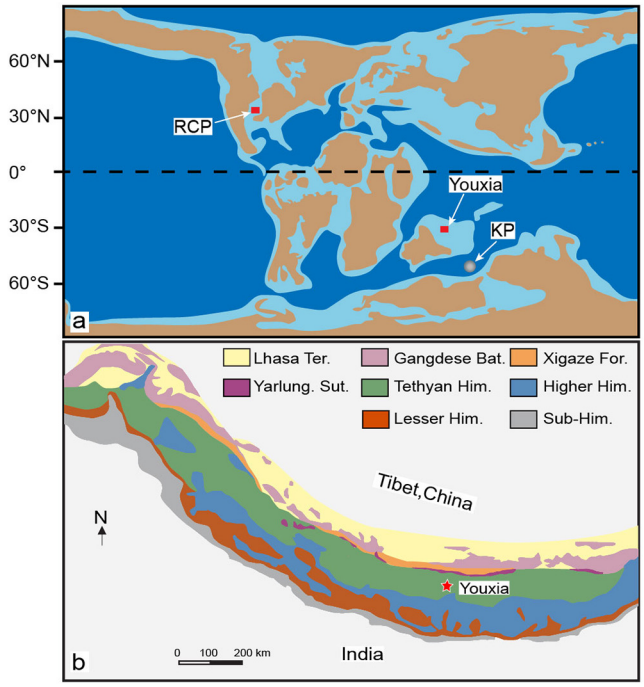

Figure 1. The location of the studied area (a) Paleographic map at latest Albian (ca. 100 Ma): time showing the location of the studied area (Youxia), Kerguelen Plateau (KP) LIPs and the Rose Creek Pit (RCP), USA (Modified from Scotese, 2016); (b) Simplified geological map of the southern Tibet and the location of the Youxia section (Modified from An et al., 2017). Lhasa Ter. — Lhasa Terrane, Gangdese Bat. — Gangdese Batholith, Xigaze For. — Xigaze Forarc Basin, Yarlung Sut. — Yarlung-Zangbo Suture Zone, Tethyan Him. — Tethyan Himalaya, Higher Him. — Higher Himalaya, Lesser Him. — Lesser Himalaya, Sub-Him. — Sub-Himalaya.

Mercury (Hg) can be a useful indicator of LIP events (e.g., Grasby et al., 2019; Shen et al., 2020). Volcanoes emit large amounts of Hg, which undergoes global transport prior to deposition into oceans (Selin, 2009). Transient Hg emission events, related to LIPs eruptions are documented throughout the Phanerozoic marine sediments (e.g., Grasby et al., 2019 and references therein). Hg isotope ratios further serve as a powerful proxy for understanding the geochemical fates of Hg (e.g., Grasby et al., 2017, 2019). Here we test if OAE 1d was also coeval with LIP activity, or represents an anomaly compared to other OAE events. We examined the Hg content and Hg isotope composition across OAE 1d in the Youxia section of the eastern Tethys (Figure 1) and discuss how changes in these proxies can be related to LIP volcanism.

2. Geological Setting

Tectonically, southern Tibet is mainly composed of five distinct zones (Figure 1b): the Higher Himalayan Crystalline Belt, the Tethyan Himalaya tectonic zone, the Indus-Yarlung Zangbo suture, the Xigaze forearc basin, and the Gandese Arc (Gansser, 1991). Cretaceous marine deposits in southern Tibet are mainly exposed in the Tethyan Himalaya tectonic zone which formed the northern margin of the Indian continent during the Early Cretaceous (Figure 1a, Hu et al., 2010).

The Tethyan Himalaya sedimentary sequence is generally subdivided into southern and northern zones, separated by the Gyirong-Kangmar Thrust (Ratschbacher et al., 1994). The studied Youxia section crops out in the Tingri area of the southern Tethyan Himalaya zone in southern Tibet (Figure 1). In the Tingri area, ~600 m of gray marls and marly limestones of late Albian-early Coniacian age were deposited in a pelagic to a hemipelagic environment of an open marine basin without prominent tectonic activity (Willems et al., 1996). The lithology of the upper Albian-lower Turonian portion of the ~150-m-thick Youxia section is dominated by fine-grained hemipelagic calcareous shales, marls, and limestones.

3. Materials and Methods

Volcanic emissions are a major natural source of Hg to the environment (Pyle & Mather, 2003). The relatively long atmospheric residence time of gaseous elemental Hg (0.5–2 years, Amos et al., 2013) allows it to be distributed globally and preserved in sedimentary records. Sedimentary Hg is generally associated with organic matter or reduced sulfur compounds (Grasby et al., 2017; Ravichandran, 2004; Sanei et al., 2012; Shen et al, 2019a, 2020; Them et al., 2019) and, more rarely, clay minerals (Kongchum et al., 2011) or Mn-Fe-oxides (Quémerais et al., 1998). Changes in redox and associated mineralization of pyrite could also affect the Hg content of sediments (Sanei et al., 2012; Shen et al., 2019b; Them et al., 2019). Recent studies highlight that Hg stable isotopes can distinguish the source of an Hg anomaly and help eliminate other alternative interpretations instead of the volcanic source (e.g., Grasby et al., 2017, 2019; Shen et al., 2019c, 2019d). Mercury isotopes undergo large mass-dependent and mass-independent fractionations (MDF and MIF) in nature and can be used to trace Hg sources and cycling rather than diagenetic effects (Blum et al., 2014).

Yao et al. (2018) combined biostratigraphic, carbon isotope stratigraphic and cyclostratigraphic studies of the lowermost ~30 m of the Youxia section to provide a composite OAE 1d record. The same samples are used here for analysis of TOC (total organic carbon) content, as well as Hg, major and trace element concentrations, and Hg isotopes. Detailed descriptions of analytical methods and the complete data set are in the supporting information Text S1, Tables S2 and S3.

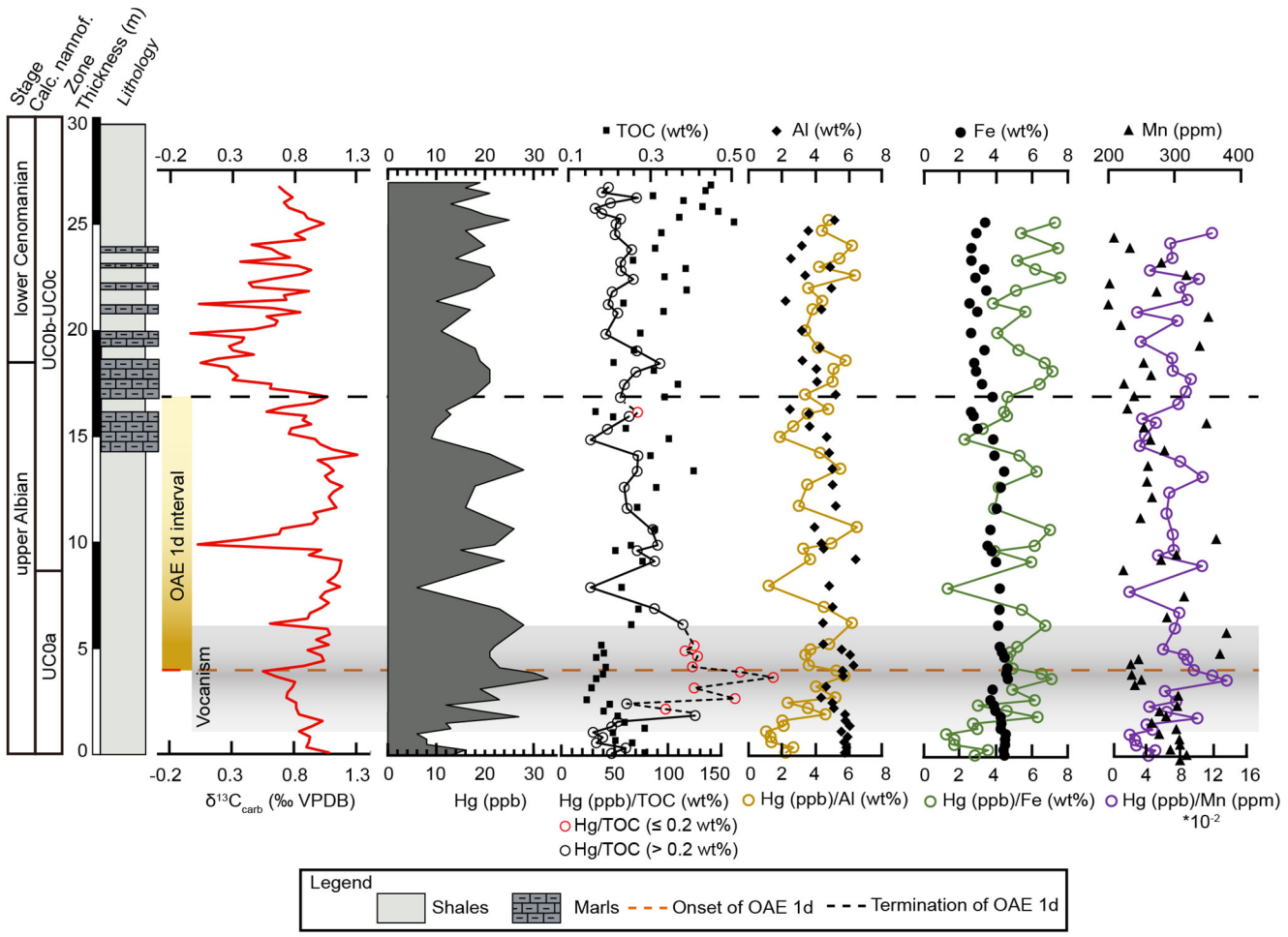

Figure 2. THg concentrations (ppb), TOC concentrations (wt%), Hg/TOC (ppb/wt%), Al concentrations (wt%), Hg/Al (ppb/wt%), Fe concentrations (wt%), Hg/Fe (ppb/wt%), Mn concentrations (ppm) and Hg/Mn (ppb/ppm) of the Youxia section. The gray shade area indicates the period with an enhanced volcanism. Calcareous nannofossil biostratigraphy and $\delta^{13}C_{carb}$ is based on Yao et al. (2018). Calc. nannof. — calcareous nannofossil. VPDB — Vienna Peedee belemnite. TOC, total organic carbon.

4. Hg Chemostratigraphy

Overall Hg concentrations at the Youxia section are lower than average for sedimentary rocks (Grasby et al., 2019). However, Hg shows a distinctive increasing trend through the interval just prior to OAE 1d (Figure 2). Two Hg peaks occur, one (from 6 to 33 ppb) is right before the onset of OAE 1d and the other (from 6 to 28 ppb) is within the OAE 1d interval (Figure 2). Hg is typically scavenged by organic matter (OM) and it is transferred into marine sediments by organo-Hg complexes (Grasby et al., 2019; Sanei et al., 2012). The strong affinity of Hg with organic matter makes it necessary to also report Hg/TOC values when identifying Hg anomalies (Sanei et al., 2012). TOC values vary within 0.15%–0.51%, most of which are higher than 0.2%, throughout the studied section (Table S2, Figure 2). TOC values show a gradual decrease up section, from 0 to 2.6 m, and then an increase to 13.5 m. After normalizing Hg concentrations with TOC values to account for Hg drawdown by organic matter (Sanei et al., 2012), a spike of Hg/TOC ratio (192 ppb/wt%) just prior to the onset of OAE 1d remains preserved but the Hg peak within OAE 1d interval disappeared, which means the latter is driven by the increase of organic matter content (Figure 2). The Hg/TOC spike is nearly three times higher than the average value of all Hg/TOC ratios of 69 ppb/wt%. We further excluded the Hg/TOC ratios of which TOC values are <0.2% to avoid artificial Hg/TOC spikes caused by low TOC (Grasby et al., 2019). Afterward, the maximum Hg/TOC value is 121 (ppb/wt%) and the Hg/TOC spike still exists (Figure 2). The Hg/TOC ratios during the OAE 1d (25–123 ppb/wt%) are also still higher than after OAE 1d (30–89 ppb/wt%). The correlation between Hg concentrations and TOC contents varies in

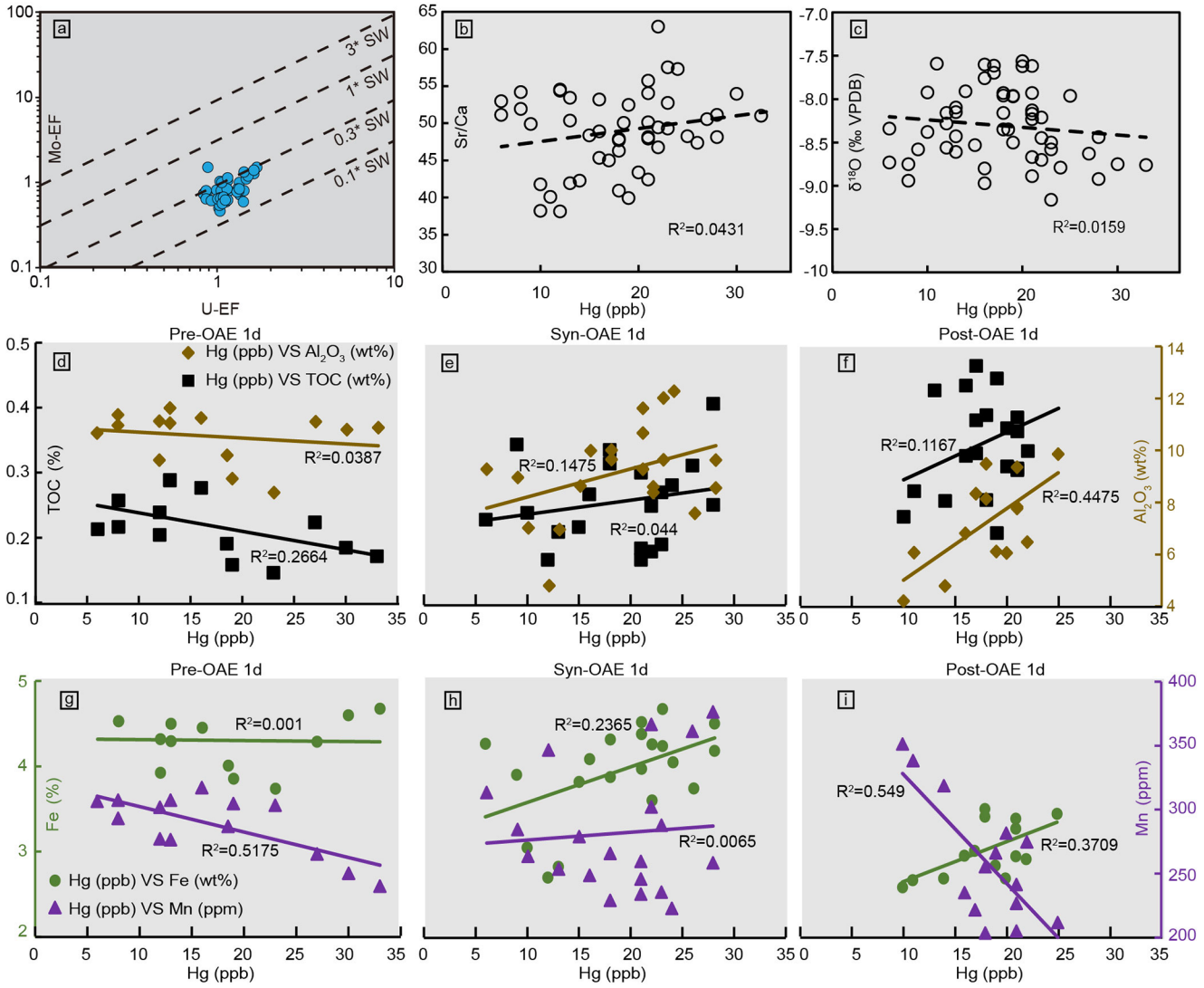

Figure 3. Comprehensive cross-plots of proxies used in this study. (a) Mo-EFs versus U-EFs for samples from the Youxia section, indicating a prominent oxic to suboxic water condition; (b) and (c) Hg concentrations versus Sr/Ca ratios and $\delta^{18}O$ values which are indicators of the diagenesis of the ancient sediments; (d) to (i) Hg concentrations versus TOC concentrations (wt%), Al concentrations (wt%), Fe concentrations (wt%) and Mn concentrations (ppm) in the different stages of OAE 1d in the Youxia section. EF, enrichment factor; TOC, total organic carbon.

different stages of the OAE 1d, such as Pre-OAE 1d (0–3.85 m), Syn-OAE 1d (3.85–16.85 m) and Post-OAE 1d (16.85–26.8 m) (Figures 3d–3f). The Hg concentrations and TOC values show poor negative correlation ($R^2 = 0.2664$) in the Pre-OAE 1d, extremely poor positive correlation ($R^2 = 0.044$) in the Syn-OAE 1d and poor positive correlation ($R^2 = 0.1167$) in the Post-OAE 1d. These results indicate that fluctuations in TOC are not controlling the Hg levels in our section. While recent studies highlight the impacts of intense weathering and post depositional organic-matter degradation on the Hg/TOC proxy in marine sediments (Charbonnier et al., 2020) our samples were collected from the fresh part of the outcrop and weathering surface has been removed before chemical analyses. Alteration can also be tested by the Sr/Ca ratio and $\delta^{18}O$ values of ancient marine sediments that may be altered significantly in cases of major change in carbonate precipitation rate (Lorens, 1981; Watkins et al., 2014), or during extensive carbonate diagenesis (Swart, 2015). The fact that there is insignificant co-variation between Hg contents and these two proxies (Figures 3b and 3c) indicates that neither process is responsible for the observed excursions in Hg content.

Clay minerals can also scavenge Hg in the water column through adsorption and subsequent deposition on the seafloor (Grasby et al., 2019). The Al_2O_3 concentration shows a gradual decrease from the bottom to the

top of the Youxia section (Figure 2). Clay mineral affects can be assessed by the Hg/Al_2O_3 ratio (ppb/wt%), which at the Youxia section also shows an increasing trend before the onset of OAE 1d and fluctuations at high values during and after OAE 1d interval (Figure 2). The Hg/Al_2O_3 ratios show a five-fold increase (0.57–3.1 ppb/wt%) during the Pre-OAE 1d interval. The low correlation coefficients of Hg concentrations with Al_2O_3 contents in the Pre-OAE 1d ($R^2 = 0.0387$; Figure 3d) also indicate that Hg enrichments are not influenced by clay mineral content. The positive correlations of Hg concentrations with Al_2O_3 and increased correlation coefficients in the Syn-OAE 1d ($R^2 = 0.1475$; Figure 3e) and Post-OAE 1d ($R^2 = 0.4475$; Figure 3f) suggest that the fluctuations at high values of Hg/Al_2O_3 during and after OAE 1d interval may be associated with clay minerals adsorption.

Redox variations can also contribute to sedimentary Hg enrichments (e.g., Shen et al., 2019b). The paleo-oxygen level of the depositional environment can be derived from some trace element indices, such as Mo-U enrichment factors (EFs, Algeo & Liu, 2020; Algeo & Tribovillard, 2009). The differences in the geochemical behavior of U and Mo, initially observed in different modern marine oxygen-depleted settings, are used to provide insight into the degree of water-mass restriction and the importance of water-column particulate shuttles (Algeo & Tribovillard, 2009). The samples from the OAE 1d intervals exhibit no enrichment of Mo (EF = 0.8–1.7) and U (EF = 0.5–1.5) (Figure 3a). These samples also exhibit lower $(Mo/U)_{auth}$ ratios of 0.1–0.3 × SW and plot on the vector in the direction of the oxic to the suboxic field (predominantly oxic). The oxic to suboxic bottom water condition would exclude the impact of reduced sulfur on the Hg enrichments (Hg-sulfide complexes, Sanei et al., 2012; Shen et al., 2019a; Them et al., 2019). Moreover, under oxic conditions, the trace elements show a strong affinity to Mn-Fe-oxyhydroxide (Algeo & Tribovillard, 2009). Hg also shows correlations with Mn-Fe-oxyhydroxide (Shen et al., 2020). After normalizing Hg contents with Fe contents, the Hg/Fe (ppb/wt%) show a remarkable increase (1.8–6.5 ppb/wt%) during the Pre-OAE 1d interval and fluctuations at high values during the Syn- and Post-OAE 1d intervals (Figure 2). However, after normalization with Mn contents, a significant Hg/Mn (ppb/ppm) spike exists in the Pre-OAE 1d interval (Figure 2). According to the cross-plots, during the Pre-OAE 1d, the Hg content shows moderate to strong negative correlation ($R^2 = 0.5175$) with the Fe content and extremely poor positive correlation ($R^2 = 0.001$) with the Mn content, which suggest that the Hg enrichments in the interval are not derived from the Mn-Fe-oxyhydroxide scavenging. The correlations of Hg contents with Fe contents exhibit gradually increased relationships from the Syn-OAE 1d ($R^2 = 0.2365$) to Post-OAE 1d ($R^2 = 0.3709$) intervals, which indicates, after the onset of OAE 1d, the Fe-oxyhydroxides is a major host of Hg. However, Hg contents still show an extremely poor positive correlation ($R^2 = 0.0065$) with Mn contents in the Syn-OAE 1d and moderate to strong negative correlation ($R^2 = 0.549$) in the Post-OAE 1d. This indicates that the change of the Hg content has no relationship with Mn-oxyhydroxide variations. In summary, all the evaluations of correlations between Hg contents and other host phases above suggest before the onset of OAE 1d that Hg is not affected by variations in organic matter and clay mineral absorptions, sulfide accumulations, redox conditions and the "shuttle" effect of Mn-Fe-oxyhydroxides. However, when the OAE 1d started, the Hg enrichments show gradually increased relationships with some of the contributors mentioned above.

Mercury isotopes are excellent tracers of the deposition pathways to marine sediments. In the Youxia section, background $\delta^{202}Hg$ values of ~−0.8 ‰ (Figure 2 and Table S3) are consistent with pre-anthropogenic marine sediments ($\delta^{202}Hg$ of −0.76‰ ± 0.16‰; Grasby et al., 2019), and the relatively narrow $\delta^{202}Hg$ values (~−0.60‰) of most geogenic sources (Yin et al., 2016). However, Hg released into the environment can experience many complicated physical, chemical, and biological reactions, which may lead to ambiguous interpretations (Blum et al., 2014), we therefore do not interpret MDF $\delta^{202}Hg$ signatures here and focus instead on MIF $\Delta^{199}Hg$ signatures of these data. On geological timescales, Hg emitted by volcanoes or derived from geogenic sources has no MIF ($\Delta^{199}Hg$ = 0 ‰; Yin et al., 2016; Zambardi et al., 2009). However, the MIF signature of geogenic Hg can be altered by aqueous Hg photoreduction in cloud droplets and surface waters, which imparts positive $\Delta^{199}Hg$ values in the residue Hg^{2+} phase and negative $\Delta^{199}Hg$ values in Hg° (g) (Bergquist & Blum, 2007). Precipitation and seawater, which contain Hg^{2+} species, are characterized by positive $\Delta^{199}Hg$ (Blum et al., 2014). Terrestrial reservoirs (e.g., vegetation, soil as well as wildfires), which primarily accumulate Hg° (g) are characterized by negative $\Delta^{199}Hg$ values (Demers et al., 2013; Them et al., 2019). Due to the difference, marine sediments that mainly receive Hg through terrestrial runoff tend to have negative $\Delta^{199}Hg$ values, whereas oceanic sediments that mainly receive atmospheric Hg^{2+} deposition tend to have positive $\Delta^{199}Hg$ values. In the Youxia section, the $\Delta^{199}Hg$ value increase from 0.04 to 0.29 ‰

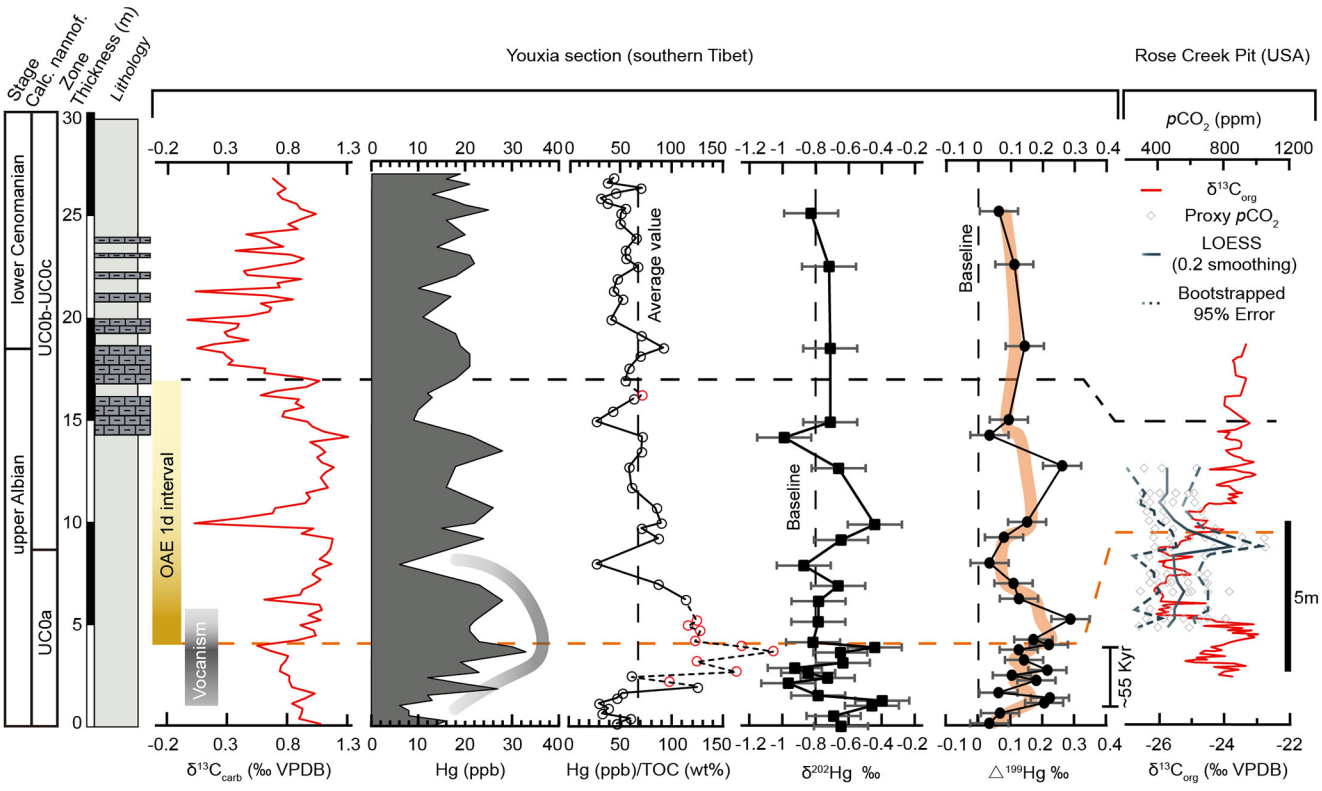

Figure 4. Geochemical plots of THg concentrations (ppb), Hg/TOC (ppb/wt%) ratios, δ^{202}Hg and Δ^{199}Hg values in the Youxia section. High-resolution multi-proxy pCO_2 reconstruction for the onset of OAE 1d was established by Richey et al. (2018). The black dashed line in the Hg/TOC (ppb/wt%) curve shows the average values of Hg/TOC ratios. Black dashed lines in δ^{202}Hg and Δ^{199}Hg curves show the baselines and represents the background values. Yellow translucent bold line represents the 3-point moving average result of Δ^{199}Hg value. Calc. nannof. — calcareous nannofossil. VPDB — Vienna Peedee belemnite. Legends according to Figure 2. OAE, Oceanic Anoxic Event; TOC, total organic carbon.

during the pre-OAE 1d and earliest OAE 1d interval (Figure 4). Although the maximum Δ^{199}Hg value does not correspond to the maximum Hg value, it is obvious that during the Hg spike interval indicated by elevated Hg content and Hg/TOC ratios, the Δ^{199}Hg value shows a steady increasing trend. The increase of Δ^{199}Hg during the Hg spike interval may be linked to one or both of the following processes: (1) a dominant contribution of direct atmospheric deposition of volcanically derived Hg^{2+}, and/or (2) increases in organic matter drawdown which effectively captures Hg (II) with positive Δ^{199}Hg signals. The first process seems the most reasonable in our study, as the latter process is not supported by the presence of correlation between Hg and TOC concentrations (Figures 3d–3f). Grasby et al. (2017) compared the Δ^{199}Hg data of sediments deposited in deep-water with a shallower marine section for the Latest Permian Extinction (LPE) and suggested that the deep-water environment is characterized by direct atmosphere deposition of volcanically derived Hg^{2+}. This is analogous to the inner shelf sediments in the Youxia section and further excludes the influence of another source such as coal, with positive Δ^{199}Hg values (Them et al., 2019). Thus, Δ^{199}Hg values of the Youxia section indicate during the latest Albian-earliest Cenomanian transition direct atmospheric deposition of volcanically derived Hg^{2+} is the prominent pathway for the Hg accumulation, and that there was increased volcanism before the onset of OAE 1d in the southern part of eastern Tethys Sea.

5. Environmental Perturbations

The Cretaceous is marked by several positive high-amplitude carbon isotope excursions that record changes in the carbon cycle and global climate (Jenkyns, 2010). Sedimentary Hg anomalies have been utilized in studies of these carbon cycle perturbations to confirm a link between major environmental perturbations and LIP eruptions, such as the Ontong Java LIP with OAE 1a, the southern Kerguelen Plateau with OAE 1b,

the Pacific or High Arctic LIPs with OAE 2 (Percival et al., 2018 and references therein). For OAE1d, there has been no definitive linkage with a driver for the event nor a previous Hg study.

Reconstruction of SSTs in the Atlantic and western Tethys realm support that enhanced volcanism led to rapid warming at onset of OAE 1d (Bottini & Erba, 2018 and references therein). At ODP Site 1052E in the western tropical Atlantic Ocean, an increase in seawater temperatures of ~1 °C, and convergence of surface and intermediate depth water temperatures, occurred just prior to the onset of OAE 1d, as calculated by foraminifera $\delta^{18}O_{carb}$ by Wilson & Norris (2001). Simultaneous extinction of calcareous nannoorganisms adapted to specific depths in the photic zone suggest strengthened upwelling and/or deep mixing of surface and intermediate water masses just prior to OAE 1d (Watkins et al., 2005). Bornemann et al. (2005) also used nannofossil temperature indices (TI) and $\delta^{18}O_{carb}$ data of the Niveau Breistroffer level to reconstruct the SSTs during OAE 1d in SE France. These data show a similar trend of increased SSTs just prior to OAE 1d. According to Bottini and Erba (2018), the $\delta^{18}O_{carb}$ curve derived from Gambacorta et al. (2015) and TI data of the Monte Petrano and Le Brecce sections at Umbria-Marche Basin, Italy, show an increase of SSTs and relative warming just preceding OAE 1d as well. The similarity of western Tethys and western tropical Atlantic Ocean paleotemperature fluctuations during OAE 1d with nannofossil-based records indicated that these paleoenvironmental changes were not local, but instead were affecting the oceans at supra-regional to global scale (Bottini & Erba, 2018).

Many studies highlight that warm temperatures are attributed to increasing atmospheric CO_2 (Anagnostou et al., 2016 and references therein). A substantial increase of atmospheric CO_2 preceding the positive CIE of OAE 1d has been reported in Rose Creek Pit (RCP), USA (Figure 1), using multi-proxy pCO_2 reconstruction methods (Figure 4; Richey et al., 2018). The reconstructed magnitude of CO_2 increase (~357 ± 150 ppm) prior to the onset of OAE 1d is similar to that of OAE 2 (150–600 ppm) but smaller in magnitude than that of OAE 1a (600–1,400 ppm) and the T-OAE (750–1,750) (Richey et al., 2018). To assess the relative connection of these OAE CO_2 events to volcanism, we amalgamated all Hg/TOC anomaly data from previous OAEs studies and calculated the enrichment factors (EFs = Maximum value/mean background value) (Table S1). The Hg/TOC EF of OAE 1d is ~3.93 which is similar to that of Weissert event (2.38–3.87), OAE 1a (2.8–4) and OAE 2 (2.92–5.92) and smaller than that of T-OAE (0.58–30.47) and OAE 1b (11.47). In addition, OAE 1d displays similar behaviors to OAE 1a and T-OAE, in that the maximum rise in pCO_2 occurs well into the negative $\delta^{13}C$ excursion and the out-of-phase relationship between changes in pCO_2 and geochemistry (Richey et al., 2018 and references therein). These similarities suggest a shared causal or developmental mechanism with OAE 1a and the OAE 2. The trigger of Weissert event, OAE 1a, OAE 1b, OAE 2 and T-OAE have all been attributed to LIP volcanism (Percival et al., 2018 and references therein). Thus, elevated atmospheric CO_2 prior to OAE 1d with an associated SST increase, combined with our Hg data, suggests that analogous to other global OAEs, the trigger of OAE 1d is also LIP volcanism.

During the Albian-Cenomanian transition, the recorded LIP volcanism includes the Caribbean LIP (100–87 Ma; Luzieux et al., 2006), the High Arctic LIP (130–80 Ma; Naber et al., 2020; Polteau et al., 2016), the Ontong Java LIP (119–25 Ma; Bryan & Ernst, 2008) and the Kerguelen LIP (130 Ma to now; Coffin et al., 2002). The Kerguelen LIP is the closest one to our study area, along the northern margin of the Indian Plate. The Central Kerguelen hotspot, with a mean plateau age of 100.4 ± 0.7 Ma, had an estimated magma output of 0.9 km^3/yr, the highest rate in the 130 Ma history of the Kerguelen Plateau (Coffin et al., 2002). OAE 1 d occurred prior to the Albian-Cenomanian boundary (~100.5 Ma). Based on the established orbital timescale by Yao et al. (2018), the duration of complete OAE 1d is ~233 kyr, and the time from the beginning of volcanism to the onset of OAE 1d is estimated to be ~55 kyr. Therefore, the intense volcanism of the Central Kerguelen hotspot is the most likely LIP activity, although other LIPs can also contribute to the Hg anomaly in this study, that served also as the source of the Hg anomaly that preceded OAE 1d. One caveat to our study is that the duration of the pre-volcanic interval (0–1 m; Figure 2) is estimated to be ~20 kyr (Yao et al., 2018), which may be not long enough to capture the whole volcanic interval. Thus, further investigations on other OAE 1d records are required.

The maximum Hg concentration in our carbonate dominated section (33 ppb) is lower than the 62.4 ppb mean in sedimentary rocks (dominantly shales, Grasby et al., 2019), and carbonates are known to have lower Hg content. The Hg concentrations though show increases above local background and the Hg/TOC ratio increasing 3–4 times above background. A similar phenomenon was observed in OAE 2 Hg records

(Percival et al., 2018 and references therein). For OAE 2 elevated Hg concentrations and Hg/TOC ratios appear in only a few records and with a low magnitude of perturbation. This observation was suggested by Percival et al. (2018) to reflect submarine LIP having mercury emitted directly into the ocean which greatly limits global distribution compared to subaerial eruptions. Hg contents, Hg/TOC ratios, Δ^{199}Hg values, and the similar Hg/TOC EFs and changing magnitude of the atmospheric pCO_2 during OAE 1d and OAE 2 all strongly support this model that submarine Hg emissions were only regional in their impact, although LIP volcanism still resulted in global environment perturbations related to elevated atmospheric pCO_2 driving increased surface and intermediate water temperatures and elevated mixing of upper ocean water that triggered the global OAE 1d.

6. Conclusions

Our study provides the first evidence of increased Hg deposition prior to OAE 1d. The absence of correlation between Hg concentrations and OMs, Mn-Fe-oxyhydroxides and/or clay minerals, the Hg content spike and overall positive Δ^{199}Hg excursion prior to the onset of OAE 1d indicate a volcanic origin rather than via scavenging organic matter and/or increase in runoff processes. The atmospheric pCO_2 reconstruction showing a major increase before the positive CIE of OAE 1d and the increase of surface and intermediate water temperature and the elevated mixing of upper ocean water in the western Tethys and the Atlantic Ocean support LIP volcanism prior to the onset of OAE 1d. According to the mean eruption age of the Central Kerguelen Plateau (100.4 ± 0.7 Ma), we suggest that the intense central portion of Kerguelen LIP volcanism may serve as the source of the Hg anomaly in the northern margin of the Indian continent and the trigger of OAE 1d global environment perturbations. As the eruption was largely submarine, the Hg signature appears more subdued than those related to subaerial LIP events. Our results add OAE 1d to the list of global events driving by enhanced CO_2 emissions by volcanic activity.

Data Availability Statement

The authors confirm that the data supporting the findings of this study are available within the supporting information and archived in the PANGAEA data repository at https://doi.pangaea.de/10.1594/PANGAEA.

Acknowledgments
The authors are grateful for the support of Dr. Huimin Liang, Xinyu Qian, Kaibo Han, Yi Zou (all at CUGB) in sampling. This work has been funded by the National Natural Science Foundation of China (Grant No. 41888101, 41672104) and China Geological Survey (Grant No. DD20190057).

References

Algeo, T. J., & Liu, J. (2020). A re-assessment of elemental proxies for paleoredox analysis. *Chemical Geology*, *540*, 119549. https://doi.org/10.1016/j.chemgeo.2020.119549

Algeo, T. J., & Tribovillard, N. (2009). Environmental analysis of paleoceanographic systems based on molybdenum–uranium covariation. *Chemical Geology*, *268*(3), 211–225. https://doi.org/10.1016/j.chemgeo.2009.09.001

Amos, H. M., Jacob, D. J., Streets, D. G., & Sunderland, E. M. (2013). Legacy impacts of all-time anthropogenic emissions on the global mercury cycle. *Global Biogeochemical Cycles*, *27*(2), 410–421. https://doi.org/10.1002/gbc.20040

Anagnostou, E., John, E. H., Edgar, K. M., Foster, G. L., Ridgwell, A., Inglis, G. N., et al. (2016). Changing atmospheric CO_2 concentration was the primary driver of early Cenozoic climate. *Nature*, *533*(7603), 380. https://doi.org/10.1038/nature17423

Bergquist, B. A., & Blum, J. D. (2007). Mass-dependent and -independent fractionation of Hg isotopes by photoreduction in aquatic systems. *Science*, *318*(5849), 417–420. https://doi.org/10.1126/science.1148050

Blum, J. D., Sherman, L. S., & Johnson, M. W. (2014). Mercury isotopes in earth and environmental sciences. *Annual Review of Earth and Planetary Sciences*, *42*(1), 249–269. https://doi.org/10.1146/annurev-earth-050212-124107

Bornemann, A., Pross, J., Reichelt, K., Herrle, J. O., Hemleben, C., & Mutterlose, J. (2005). Reconstruction of short-term paleoceanographic changes during the formation of the Late Albian 'Niveau Breistroffer' black shales (Oceanic Anoxic Event 1d, SE France). *Journal of the Geological Society*, *162*(4), 623–639. https://doi.org/10.1144/0016-764903-171

Bottini, C., & Erba, E. (2018). Mid-Cretaceous paleoenvironmental changes in the western Tethys. *Climate of the Past*, *14*(8), 1147–1163. https://doi.org/10.5194/cp-14-1147-2018

Bryan, S. E., & Ernst, R. E. (2008). Revised definition of Large Igneous Provinces (LIPs). *Earth-Science Reviews*, *86*(1), 175–202. https://doi.org/10.1016/j.earscirev.2007.08.008

Charbonnier, G., Adatte, T., Föllmi, K. B., & Suan, G. (2020). Effect of intense weathering and postdepositional degradation of organic matter on Hg/TOC proxy in organic-rich sediments and its implicationsfor deep-time investigations. *Geochemistry, Geophysics, Geosystems*, *21*(2), e2019GC008707. https://doi.org/10.1029/2019gc008707

Coffin, M. F., Pringle, M. S., Duncan, R. A., Gladczenko, T. P., Storey, M., Müller, R. D., et al. (2002). Kerguelen hotspot magma output since 130 Ma. *Journal of Petrology*, *43*(7), 1121–1137. https://doi.org/10.1093/petrology/43.7.1121

Demers, J. D., Blum, J. D., & Zak, D. R. (2013). Mercury isotopes in a forested ecosystem: Implications for air-surface exchange dynamics and the global mercury cycle, *Advancing Earth and Space Science*, *27*(1), 222–238. https://doi.org/10.1002/gbc.20021

Gambacorta, G., Jenkyns, H. C., Russo, F., Tsikos, H., Wilson, P. A., Faucher, G., et al. (2015). Carbon- and oxygen-isotope records of mid-Cretaceous Tethyan pelagic sequences from the Umbria-Marche and Belluno Basins (Italy). *Newsletters on Stratigraphy*, *48*(3), 299–323. https://doi.org/10.1127/nos/2015/0066

Gansser, A. (1991). *Facts and theories on the Himalayas*. Eclogae Geologicae Helvetiae. Retrieved from https://www.semanticscholar.org/paper/Facts-and-theories-on-the-Himalayas-Gansser/9e7668272277241ef8cf33317d4f43f9449208c7

Giorgioni, M., Weissert, H., Bernasconi, S. M., Hochuli, P. A., Keller, C. E., Coccioni, R., et al. (2015). Paleoceanographic changes during the Albian–Cenomanian in the Tethys and North Atlantic and the onset of the Cretaceous chalk. *Global and Planetary Change*, *126*, 46–61. https://doi.org/10.1016/j.gloplacha.2015.01.005

Grasby, S. E., Shen, W., Yin, R., Gleason, J. D., Blum, J. D., Lepak, R. F., et al. (2017). Isotopic signatures of mercury contamination in latest Permian oceans. *Geology*, *45*(1), 55–58. https://doi.org/10.1130/g38487.1

Grasby, S. E., Them, T. R., Chen, Z., Yin, R., & Ardakani, O. H. (2019). Mercury as a proxy for volcanic emissions in the geologic record. *Earth-Science Reviews*, *196*. https://doi.org/10.1016/j.earscirev.2019.102880

Hu, X., Jansa, L., Chen, L., Griffin, W. L., O'Reilly, S. Y., & Wang, J. (2010). Provenance of Lower Cretaceous Wölong Volcaniclastics in the Tibetan Tethyan Himalaya: Implications for the final breakup of Eastern Gondwana. *Sedimentary Geology*, *223*(3–4), 193–205. https://doi.org/10.1016/j.sedgeo.2009.11.008

Jenkyns, H. C. (2010). Geochemistry of oceanic anoxic events. *Geochemistry, Geophysics, Geosystems*, *11*(3), 427–428. https://doi.org/10.1029/2009GC002788

Kongchum, M., Hudnall, W. H., & Delaune, R. D. (2011). Relationship between sediment clay minerals and total mercury. *Journal of Environmental Science and Health*, *46*(5), 534–539. https://doi.org/10.1080/10934529.2011.551745

Leckie, R. M., Bralower, T. J., & Cashman, R. (2002). Oceanic anoxic events and plankton evolution: Biotic response to tectonic forcing during the mid-Cretaceous. *Paleoceanography*, *17*(3), 1311–1329. https://doi.org/10.1029/2001PA000623

Lorens, R. B. (1981). Sr, Cd, Mn and Co distribution coefficients in calcite as a function of calcite precipitation rate. *Geochimica et Cosmochimica Acta*, *45*(4), 553–561. https://doi.org/10.1016/0016-7037(81)90188-5

Luzieux, L. D. A., Heller, F., Spikings, R., Vallejo, C. F., & Winkler, W. (2006). Origin and Cretaceous tectonic history of the coastal Ecuadorian forearc between 1°N and 3°S: Paleomagnetic, radiometric and fossil evidence. *Earth and Planetary Science Letters*, *249*(3), 400–414. https://doi.org/10.1016/j.epsl.2006.07.008

Naber, T. V., Grasby, S. E., Cuthbertson, J. P., Rayner, N., & Tegner, C. (2020). New constraints on the age, geochemistry, and environmental impact of high Arctic Large Igneous Province magmatism: Tracing the extension of the Alpha Ridge onto Ellesmere Island, Canada. *GSA Bulletin*. https://doi.org/10.1130/B35792.1%JGSABulletin

Ogg, J. G., Hinnov, L. A., & Huang, C. (2012). Chapter 27 - Cretaceous, in *The geologic time scale*, F. M. Gradstein, J. G. Ogg, M. D. Schmitz, & G. M. Ogg (Eds)., pp. 793–853, Elsevier, Boston. Retrieved from https://www.sciencedirect.com/book/9780444594259/the-geologic-time-scale

Percival, L. M. E., Jenkyns, H. C., Mather, T. A., Dickson, A. J., Batenburg, S. J., Ruhl, M, et al. (2018). Does large igneous province volcanism always perturb the mercury cycle? Comparing the records of Oceanic Anoxic Event 2 and the End-Cretaceous to other Mesozoic events. *American Journal of Science*, *318*(8), 799–860. https://doi.org/10.2475/08.2018.01

Polteau, S., Hendriks, W. H. B., Planke, S., Ganerød, M., Corfu, F., Faleide, J. I., et al. (2016). The Early Cretaceous Barents Sea sill complex: Distribution, 40Ar/39Ar geochronology, and implications for carbon gas formation. *Palaeogeography, Palaeoclimatology, Palaeoecology*, *441*, 83–95. https://doi.org/10.1016/j.palaeo.2015.07.007

Pyle, D. M., & Mather, T. A. (2003). The importance of volcanic emissions for the global atmospheric mercury cycle. *Atmospheric Environment*, *37*(36), 5115–5124. https://doi.org/10.1016/j.atmosenv.2003.07.011

Quémerais, B., Cossa, D., Rondeau, B., Pham, T. T., & Fortin, B. (1998). Mercury distribution in relation to iron and manganese in the waters of the St. Lawrence river. *The Science of the Total Environment*, *213*(1), 193–201. https://doi.org/10.1016/S0048-9697(98)00092-8

Ratschbacher, L., Frisch, W., Liu, G., & Chen, C. (1994). Distributed deformation in southern and western Tibet during and after the India-Asia collision. *Journal of Geophysical Research: Solid Earth*, *99*(B10), 19917–19945. https://doi.org/10.1029/94jb00932

Ravichandran, M. (2004). Interactions between mercury and dissolved organic matter––A review. *Chemosphere*, *55*(3), 319–331. https://doi.org/10.1016/j.chemosphere.2003.11.011

Richey, J. D., Upchurch, G. R., Montañez, I. P., Lomax, B. H., Suarez, M. B., Crout, M. J. N., et al. (2018). Changes in CO_2 during ocean anoxic event 1d indicate similarities to other carbon cycle perturbations. *Earth and Planetary Science Letters*, *491*, 172–182. https://doi.org/10.1016/j.epsl.2018.03.035

Sanei, H., Grasby, S. E., & Beauchamp, B. (2012). Latest Permian mercury anomalies. *Geology*, *40*(1), 63–66. https://doi.org/10.1130/g32596.1

Schlanger, S. O., & Jenkyns, H. C. (1976). Cretaceous oceanic anoxic events: Causes and consequences. *Geologie en Mijnbouw*, *55*(3–4), 179–184.

Selin, N. E. (2009). Global biogeochemical cycling of mercury: A review. *Annual Review of Environment and Resources*, *34*(1), 43–63. https://doi.org/10.1146/annurev.environ.051308.084314

Shen, J., Algeo, T. J., Chen, J., Planavsky, N. J., Feng, Q., Yu, J., et al. (2019a). Mercury in marine Ordovician/Silurian boundary sections of South China is sulfide-hosted and non-volcanic in origin. *Earth and Planetary Science Letters*, *511*, 130–140. https://doi.org/10.1016/j.epsl.2019.01.028

Shen, J., Algeo, T. J., Planaysky, N. J., Yu, J., Feng, Q., Song, H., et al. (2019b). Mercury enrichments provide evidence of Early Triassic volcanism following the End-Permian mass extinction. *Earth-Science Reviews*, *195*, 191–212. https://doi.org/10.1016/j.earscirev.2019.05.010

Shen, J., Chen, J., Algeo, T. J., Yuan, S., Feng, Q., Yu, J., et al. (2019c). Evidence for a prolonged Permian–Triassic extinction interval from global marine mercury records. *Nature Communications*, *10*(1), 1563. https://doi.org/10.1038/s41467-019-09620-0

Shen, J., Feng, Q., Algeo, T. J., Liu, J., Zhou, C., Wei, W., et al. (2020). Sedimentary host phases of mercury (Hg) and implications for use of Hg as a volcanic proxy. *Earth and Planetary Science Letters*, *543*, 116333. https://doi.org/10.1016/j.epsl.2020.116333

Shen, J., Yu, J., Chen, J., Algeo, T. J., Xu, G., Feng, Q., et al. (2019d). Mercury evidence of intense volcanic effects on land during the Permian-Triassic transition. *Geology*, *47*(12), 1117–1121. https://doi.org/10.1130/G46679.1%JGeology

Sinton, C. W., & Duncan, R. A. (1997). Potential links between ocean plateau volcanism and global ocean anoxia at the Cenomanian-Turonian boundary. *Economic Geology and the Bulletin of the Society of Economic Geologists*, *92*(7–8), 836–842. https://doi.org/10.2113/gsecongeo.92.7-8.836

Swart, P. K. (2015). The geochemistry of carbonate diagenesis: The past, present and future. *Sedimentology*, *62*(5), 1233–1304. https://doi.org/10.1111/sed.12205

Them, T. R., Jagoe, C. H., Caruthers, A. H., Gill, B. C., Grasby, S. E., Gröcke, D. R., et al. (2019). Terrestrial sources as the primary delivery mechanism of mercury to the oceans across the Toarcian Oceanic Anoxic Event (Early Jurassic). *Earth and Planetary Science Letters*, *507*, 62–72. https://doi.org/10.1016/j.epsl.2018.11.029

Watkins, D. K., Cooper, M. J., & Wilson, P. A. (2005). Calcareous nannoplankton response to late Albian oceanic anoxic event 1d in the western North Atlantic. *Paleoceanography*, *20*(2). https://doi.org/10.1029/2004PA001097

Watkins, J. M., Hunt, J. D., Ryerson, F. J., & DePaolo, D. J. (2014). The influence of temperature, pH, and growth rate on the δ18O composition of inorganically precipitated calcite. *Earth and Planetary Science Letters*, *404*, 332–343. https://doi.org/10.1016/j.epsl.2014.07.036

Weissert, H. (1989). C-Isotope stratigraphy, a monitor of paleoenvironmental change: A case study from the early cretaceous. *Surveys in Geophysics*, *10*(1), 1–61. https://doi.org/10.1007/bf01901664

Willems, H., Zhou, Z., Zhang, B., & Gräfe, K.-U. (1996). Stratigraphy of the upper cretaceous and lower tertiary strata in the Tethyan Himalayas of Tibet (Tingri area, China). *Geologische Rundschau*, *85*(4), 723. https://doi.org/10.1007/bf02440107

Wilson, P. A., & Norris, R. D. (2001). Warm tropical ocean surface and global anoxia during the mid-Cretaceous period. *Nature*, *412*(6845), 425–429. https://doi.org/10.1038/35086553

Yao, H., Chen, X., Melinte-Dobrinescu, M. C., Wu, H., Liang, H., & Weissert, H. (2018). Biostratigraphy, carbon isotopes and cyclostratigraphy of the Albian-Cenomanian transition and Oceanic Anoxic Event 1d in southern Tibet. *Palaeogeography, Palaeoclimatology, Palaeoecology*, *499*, 45–55. https://doi.org/10.1016/j.palaeo.2018.03.005

Yin, R., Feng, X., Hurley, J. P., Krabbenhoft, D. P., Lepak, R. F., Kang, S., et al. (2016). Historical records of mercury stable isotopes in sediments of Tibetan Lakes. *Scientific Reports*, *6*(1), 23332. https://doi.org/10.1038/srep23332

Zambardi, T., Sonke, J. E., Toutain, J. P., Sortino, F., & Shinohara, H. (2009). Mercury emissions and stable isotopic compositions at Vulcano Island (Italy). *Earth and Planetary Science Letters*, *277*(1–2), 236–243. https://doi.org/10.1016/j.epsl.2008.10.023